Analysis of the Decadal and Interdecadal Variations of the East Asian Winter Monsoon as Simulated by 20 Coupled Models in IPCC AR4

HE Shengping[1,2,3]* (贺圣平) and WANG Huijun[1,3] (王会军)

1 *Nan-Zhu International Research Center, Institute of Atmospheric Physics, Chinese Academy of Sciences, Beijing* 100029

2 *Climate Change Research Center, Chinese Academy of Sciences, Beijing* 100029

3 *Graduate University of Chinese Academy of Sciences, Beijing* 100049

(Received October 28, 2011; in final form June 25, 2012)

ABSTRACT

Using the output data of 20 coupled climate models used in IPCC AR4 and observational data from NCEP, the capability of the models to simulate the boreal winter climatology of the East Asian sea level pressure, 850-hPa wind, and surface air temperature; the decadal variations of the East Asian winter monsoon (EAWM) intensity and EAWM-related circulation, and the interdecadal variations of EAWM-related circulation are systematically evaluated. The results indicate that 16 models can weakly simulate the declining trend of the EAWM in the 1980s. More than half of the models produce relatively reasonable decadal variations of the EAWM-related circulation and the interdecadal differences of EAWM-related circulation between the boreal winters of 1960–1985 and 1986–1998, including the weakened Siberian high, Aleutian low, and East Asian trough, the enhanced Arctic oscillation and North Pacific oscillation, and a deepened polar vortex. It is found that the performance of the multi-selected-model ensemble in reproducing the spatial distribution of the variations is encouraging, although the variational amplitudes are generally smaller than the observations. In addition, it is found that BCCR-BCM2.0, CGCM3.1-T63, CNRM-CM3, CSIRO-MK3.0, GISS-ER, INM-CM3.0, and MRI-CGCM2.3.2 perform well in every aspect.

Key words: IPCC AR4, East Asian winter monsoon, interdecadal variations, simulation analysis

Citation: He Shengping and Wang Huijun, 2012: Analysis of the decadal and interdecadal variations of the East Asian winter monsoon as simulated by 20 coupled models in IPCC AR4. *Acta Meteor. Sinica,* **26**(4), 476–488, doi: 10.1007/s13351-012-0407-6.

1. Introduction

With the continuous development of climate models, the validation of their simulation capacity has become an important research subject. Numerous assessments of regional and global climate simulations have been published, including a large number of studies on East Asian climate. For example, Zhao et al. (1995) assessed the performance of five coupled general circulation models (CGCMs) in simulating the climate in East Asia and China, indicating that these five CGCMs can simulate the spatial distribution of surface air temperature (SAT), precipitation, and circulation in the East Asian region reasonably well, performing best in winter and worst in summer. Subsequently, many Chinese scholars carried out similar studies (Wang and Zhang, 1999; Xu et al., 2002; Zhou and Li, 2002; Gao et al., 2003a, b, 2004; Zhao et al., 2003; Zhou et al., 2004; Feng and Fu, 2007).

Accompanying the assessment reports of the Intergovernmental Panel on Climate Change (IPCC), evaluations of the performance of coupled models in simulating the climate over East Asia have been conducted worldwide (Buhe et al., 2003; Min et al., 2004; Kripalani et al., 2007a; Jiang, 2008). Overall, most coupled models can successfully reproduce the annual

Supported by the National Natural Science Foundation of China (41130103 and 40905041), Knowledge Innovation Program of the Chinese Academy of Sciences (KZCX2-YW-QN202), and China Global Change Research Program (2012CB955401).

*Corresponding author: hshp@mail.iap.ac.cn.

and seasonal SAT and precipitation climatology of East Asia, with relatively good performance for boreal autumn and the annual mean (Jiang et al., 2005). However, discrepancies still exist among different coupled models (Wang and Xiong, 2004; Xu et al., 2007; Jiang et al., 2009). It has been found that the ability of coupled models to simulate SAT is generally better than that of precipitation, with lower simulated temperature and higher simulated precipitation as compared to the observation. Coupled models not only reproduce SAT climatology reasonably well, but also perform well in simulating the interannual variability of the global and the Northern Hemispheric mean SAT, with a relatively poorer but acceptable performance for China (Zhou and Yu, 2006). However, their performance in simulating precipitation is not poor.

Although most coupled models show a relatively realistic representation of monsoon precipitation climatology, the interannual and interdecadal variations of simulations are rarely comparable with observations (Dai, 2006; Annamalai et al., 2007; Liu and Jiang, 2009; Gu and Li, 2010). There are many assessments on coupled models, focusing mostly on simulations of the East Asian monsoon and South Asian monsoon precipitation climatology and intraseasonal and interannual monsoon variations (Lambert and Boer, 2001; Lin et al., 2006; Kripalani et al., 2007b; Lin et al., 2008; Sun and Ding, 2008; Bollasina and Nigam, 2009). By contrast, few studies have specifically performed assessments of East Asian winter monsoon (EAWM) simulations, especially with regard to its decadal and interdecadal variations. It is known that the variability of the EAWM can exert large influences on China, Korea, Japan, and surrounding regions, with profound economic and social impacts (Guo, 1994; Ji and Sun, 1997; Wang et al., 2003; Wang and Chen, 2010). Previous studies have shown that the EAWM has exhibited evident decadal and interdecadal variations over the past half century as well as a significant weakening during the mid 1980s (Yan et al., 2009; Wang and Chen, 2010). Thus, the ability of current coupled models to capture the above variations of the EAWM is also an important indication of a model's performance in East Asian climate simulations.

Based on the outputs of 20 coupled models in IPCC AR4, this paper aims to examine to what extent the current state-of-the-art coupled climate models can reproduce the observed EAWM weakening trend of the 1980s together with its climatology and interdecadal variations over the past half century.

The paper is arranged as follows. Section 2 introduces the data and analysis methods. Section 3 depicts the accuracy of the coupled models in capturing the climatology of the sea level pressure (SLP) over East Asia and the Pacific, and 850-hPa wind and SAT over East Asia. The weakening trend of the EAWM and the corresponding circulation changes from both observations and simulations are addressed in Section 4. Section 5 presents an assessment of the performance with regard to interdecadal variation simulations. A summary and discussion are given in Section 6.

2. Data and analysis method

The observational datasets used in this study are the monthly mean NCEP/NCAR (National Centers for Environmental Prediction/National Center for Atmospheric Research) reanalysis data during 1960–1998 (Kalnay et al., 1996). The 20th-century monthly mean simulations during 1960–1998 produced by coupled climate models used for the IPCC AR4, which are often called the "20th-century Climate in Coupled Models (20C3M)", are used as model data (http://www-pcmdi.llnl.gov/ipcc/about_ipcc.php). Because these models employ different horizontal resolutions, for convenience, the outputs from all models are linearly interpolated onto the same grid resolution as the observations. The SAT is interpolated to the T62 Gaussian grid with 192×94 points; the other variables are interpolated to the $2.5° \times 2.5°$ horizontal grid with 144×73 points. Seasonal means are constructed from the monthly means by averaging the data of December, January, and February (DJF) during 1960–1998. Here, our convention is that the winter of 1960 refers to the 1960/1961 winter.

To quantitatively evaluate the models' performance in simulating climatology of a specific region, two statistical variables will be used (Jiang et al., 2005). One is the regional average error (RAE):

$$\mathrm{RAE} = \overline{x} - \overline{y} = \frac{1}{n}\sum_{i=1}^{n} x_i - \frac{1}{n}\sum_{i=1}^{n} y_i, \tag{1}$$

and the other is the spatial correlation coefficient (SCC):

$$\mathrm{SCC} = \frac{\frac{1}{n}\sum\limits_{i=1}^{n}(x_i-\overline{x})(y_i-\overline{y})}{\sqrt{\frac{1}{n}\sum\limits_{i=1}^{n}(x_i-\overline{x})^2}\sqrt{\frac{1}{n}\sum\limits_{i=1}^{n}(y_i-\overline{y})^2}}, \tag{2}$$

where x_i (y_i) denotes the simulation (observation) value at the ith spatial grid point, and n is the total number of grid points within the domain.

In order to eliminate the influence of model topography differences on the surface air temperature, a revising formula is applied:

$$T = T_{\mathrm{M}} - (h_{\mathrm{M}} - h_0) \times \gamma_{\mathrm{s}}, \tag{3}$$

where T_{M} (h_{M}) is a model's SAT (topography) that has been interpolated to the T62 Gaussian grid, h_0 is the real topography, γ_{s} is the atmospheric lapse rate (–6.5 K km^{-1}), and T is the revised SAT.

Two multi-model ensemble mean methods are used in this study. One is applied to evaluating the models' performance in simulating the climatology of the EAWM, which includes all the available models. The other, which only takes into account the models whose coefficients of spatial correlation between the observed and simulated decadal and interdecadal variations exceed the 5% significance level, is used to investigate the models' ability to reproduce the decadal and interdecadal change of the EAWM-related circulation.

3. Performance assessment of the climatology simulations

The ability to reasonably reproduce observed climatology is a primary factor in judging whether a model's simulation of the interdecadal variation is credible (Sun and Ding, 2008). Thus, to obtain an overview of the models' simulation capability for East Asia, the climatology simulated by the coupled models is first validated. Considering the general characteristics of the EAWM, we investigate the validity of the simulated climatologies of the Siberian high (SH; for the domain of 20°–65°N, 70°–140°E), the Aleutian low (AL; for the domain of 30°–70°N, 150°E–120°W), the 850-hPa northwesterly flow in East Asia (for the domain of 10°–60°N, 115°–150°E), and the SAT in the region of 15°–55°N and 70°–150°E. The corresponding statistical results are listed in Table 1.

3.1 Sea level pressure

As is well known, there exists a large heat forcing contrast between the ocean and the continent due to their different thermal capacities in winter (Tao and Chen, 1987), which is clearly reflected by the SH and AL located in East Asia and North Pacific, respectively. As shown in Fig. 1a, the above-mentioned geographical distribution of the winter sea level pressure is generally reproduced by the 19-model ensemble mean (IPSL-CM4, Institute Pierre Simon Laplace Coupled Model version 4, is excluded, as will be explained later), although some deviations are inevitable. In general, sea level pressure is overestimated in the low latitudes and underestimated in the high latitudes, with regional biases from –2 to 2 hPa. The poorest performances are generally registered in high mountains, such as the Iranian Plateau, the Tibetan Plateau, the western and northern Mongolian Plateau, the Stanovoy range, the Chersky mountains, and the Alaska range, implying possible topographic effects on the simulations.

Table 1 shows that, for the SH, the RAE of the multi-model ensemble mean is only –0.003 hPa, denoting the multi-model's superiority to any single model in simulating the climatology. Furthermore, the SCC is as high as 0.934, indicating that the spatial distribution of the annual sea level pressure is well depicted by the multi-model ensemble mean for East Asia. In addition, IPSL-CM4 has the poorest performance in depicting the SH, demonstrating a false high over the Tibetan Plateau, together with a 5.566-hPa RAE and an SCC of 0.571. For this reason, IPSL-CM4 was excluded from the multi-model mean of the sea level pressure. Meanwhile, the RAE of the rest of the cou-

Table 1. Statistics of EAWM-related circulation and surface air temperature simulated by 20 coupled models

	SH (20°–65°N, 70°–140°E)		AL (30°–70°N, 50°E–120°W)		uv_{850} (10°–60°N, 115°–150°E)	u_{850}	v_{850}	SAT (15°–55°N, 70°–150°E)	
Model	RAE (hPa)	SCC	RAE (hPa)	SCC	RAE (m s^{-1})	SCC	SCC	RAE (℃)	SCC
BCCR-BCM2.0	0.480	0.928	5.403	0.911	0.306	0.989	0.849	–2.630	0.992
CCSM3	–1.175	0.739	–3.189	0.902	1.480	0.988	0.898	0.580	0.989
CGCM3.1 (T47)	1.841	0.917	–0.201	0.937	0.279	0.981	0.925	–2.116	0.975
CGCM3.1 (T63)	1.333	0.924	0.721	0.902	0.452	0.966	0.924	–1.180	0.984
CNRM-CM3	1.690	0.820	3.508	0.952	0.845	0.972	0.864	–1.186	0.983
CSIRO-MK3.0	0.535	0.781	–6.197	0.945	0.857	0.967	0.833	–2.106	0.993
CSIRO-MK3.5	–1.444	0.692	–6.815	0.916	1.346	0.963	0.818	1.550	0.994
GFDL-CM2.0	–0.628	0.816	–1.913	0.965	0.881	0.986	0.915	–3.810	0.986
GFDL-CM2.1	–0.146	0.818	0.489	0.971	1.208	0.981	0.881	–1.687	0.989
GISS-ER	0.286	0.864	–1.076	0.767	0.193	0.947	0.810	0.605	0.985
INGV-ECHAM4	–0.053	0.911	1.004	0.949	0.339	0.971	0.894	1.675	0.992
INM-CM3.0	–2.235	0.708	1.518	0.841	0.331	0.980	0.850	–2.276	0.975
IPSL-CM4	5.566	0.571	–8.168	0.940	0.521	0.952	0.869	–2.617	0.992
MIROC3.2 (medres)	–1.274	0.716	–2.287	0.889	1.154	0.984	0.895	–0.160	0.991
MIROC3.2 (hires)	–0.508	0.729	–5.183	0.940	1.345	0.982	0.892	0.412	0.994
ECHAM5/MPI-OM	–0.356	0.937	1.826	0.965	0.104	0.984	0.900	0.819	0.993
MRI-CGCM2.3.2	1.406	0.834	1.524	0.934	–0.770	0.931	0.732	0.725	0.982
PCM1	1.674	0.854	2.890	0.965	0.417	0.980	0.930	–2.181	0.986
UKMO-HadCM3	–2.277	0.823	0.071	0.883	–0.936	0.982	0.859	–1.054	0.985
UKMO-HadGEM1	0.793	0.921	3.798	0.881	–0.030	0.979	0.867	–3.489	0.973
Ensemble mean	–0.003[1]	0.934[1]	–0.216[1]	0.976[1]	0.353	0.992	0.945	–1.035	0.996

[1]IPSL-CM4 is excluded. SH: Siberian high, AL: Aleutian low, uv_{850}: resultant wind velocity at 850 hPa, u_{850}: zonal wind at 850 hPa, v_{850}: meridional wind at 850 hPa, and SAT: surface air temperature.

pled models varies from –2.3 to 1.8 hPa. Moreover, INGV-ECHAM4 (National Institute of Geophysics and Volcanology, ECHAM 4.6 Model) and ECHAM5/MPI-OM (Max Planck Ocean Model) show a better performance in simulating the sea level pressure in East Asia, with RAE (SCC) values of –0.053 (0.911) and 0.356 (0.937) hPa, respectively.

In contrast to the SH, the AL is more successfully reproduced by the individual models according to their SCC. The SCC values of 15 models exceed 0.9, with the highest reaching 0.971 (GFDL-CM2.1: Geophysical Fluid Dynamics Laboratory Climate Model version 2.1). Although GISS-ER (Goddard Institute for Space Studies, Model E20/Russell) has the lowest value (0.767), it still has an SCC superior to that of IPSL-CM4 for the SH when compared to the observations. Thus, it is noted that the current state-of-the-art coupled models exhibit better performance in simulating spatial variations over flat terrain than over complex topography. At the same time, some disagreements still exist between the simulated AL and the reanalysis data, with the RAE values from –8.168 to 5.403 hPa. However, for the multi-model ensemble mean, the decrease in RAE (–0.216 hPa) is quite notable, together with a slight increase in the SCC (0.976). All together, the above analysis reveals that the multi-model ensemble mean generally exhibits much better performance than the individual models.

3.2 Northwesterly flow in East Asia

Previous studies have indicated that the most prominent feature of the northwesterly flow along the east flank of the SH is its divarication in the south of Japan, with one branch flowing straight toward the subtropical western and central Pacific and the other flowing along the coast of East Asia (Chen et al., 2005; Wang and Chen, 2010). Figure 1b shows the 850-hPa wind climatology of the 20-model ensemble mean (vector) and the velocity difference between simulation and observation (shaded). Obviously, the 20-model ensemble mean coincides well with the above spatial pattern. However, discrepancies are also exhibited. The simulated velocity is 0.5–1.5 m s^{-1} higher than the observations over the North China Plain, the Philippines, the Yablonoi mountains, Korea, and Japan. The biases in certain areas reach up to 2 m s^{-1}. On the other hand, the velocity is underestimated by 0.5–1.5 m s^{-1} in southern China, the Northeast China Plain, the East China Sea, the West Pacific, and the Stanovoy range. Overall, the 20-model ensemble mean of 850-hPa wind agrees, to a certain extent, with the observation.

To specify the individual coupled model's capacity to simulate the 850-hPa wind, the simulated zonal wind, meridional wind, and resultant wind velocity were analyzed. As listed in Table 1, even though the RAE of the multi-model mean wind velocity is only 0.353 m s^{-1}, the multi-model ensemble did not achieve the best performance as in other cases. Comparatively, the BCCR-BCM2.0 (Bjerknes Centre for Climate Research-Bergen Climate Model version 2), CGCM3.1 (T47) (Coupled General Circulation Model version 3.1), GISS-ER, INGV-ECHAM4, INM-CM3.0 (Institute for Numerical Mathematics Climate Model version 3), ECHAM5/MPI-OM, and UKMO-HadGEM1 (Met Office Hadley Centre Global Environmental Model version 1) perform slightly better than the multi-model ensemble, with RAE values of 0.306, 0.279, 0.193, 0.339, 0.331, 0.104, and –0.030 m s^{-1}, respectively. In addition, CCSM3 (Community Climate System Model version 3), CSIRO-MK3.5 (Commonwealth Scientific and Industrial Research Organisation Mark version 3.0), GFDL-CM2.1, MIROC3.2 (medres) (Model for Interdisciplinary Research on Climate version 3.2), and MOROC3.2 (hires) give relatively poor simulations, with the RAE values reaching 1.480, 1.346, 1.208, 1.154, and 1.345 m s^{-1}, respectively.

The models' ability to simulate the East Asian zonal wind climatology is considerably robust. Of the 20 models, 18 have significant coefficients of spatial correlation with the observation, all of which exceed 0.95. The SCC of the 20-model ensemble mean is as high as 0.992. Apparently, all of the coupled models can successfully depict the spatial distribution of the zonal wind at 850 hPa in East Asia. Meanwhile, the discrepancies of the simulated meridional wind at 850 hPa are relatively pronounced. The primary manifestation is the decrease in the SCC, with only 5 models [CGCM3.1 (T47), CGCM3.1 (T63), GFDL-CM2.0, ECHAM5/MPI-OM, and PCM1 (Coupled Model Parallel Climate Model, NCAR)] achieving an SCC exceeding 0.9. Fortunately, most of the models' SCC values remain above 0.85. Additionally, the SCC of the multi-model ensemble mean is still sufficiently high, up to 0.945. Overall, although there is some disagreement between the simulated and reanalysis data, all of the coupled models can reasonably reproduce the geographical distribution and variational magnitude of the northwesterly flow at 850 hPa in East Asia.

3.3 Surface air temperature

Regardless of how the circulation changes, its influence will be reflected by variations in the surface air temperature (Chen and Sun, 1999; Gong et al., 2002; Zhao and Zhang, 2006). Thus, it is interesting and necessary to examine whether the coupled models can successfully capture the surface air temperature climatology in East Asia. As displayed in Fig. 1c, the surface air temperature simulated by the 20-model ensemble is distributed over a latitudinal band and gradually decreases northward. A large extent of cooling occurs over the Tibetan Plateau and Xinjiang Region. This spatial pattern agrees in general with the observations. However, there are also large discrepancies between the observed and simulated regional features, especially in western China, where the temperature is underestimated or overestimated by more than 4°C. Furthermore, large simulation errors arise in the Kazakhskiy Melkosopochnik and Mongolian Plateau as well. Compared with the west, the biases in the east, where the topography is much flatter, are relatively smaller.

The values included in Table 1 indicate that the state-of-the-art coupled models have the best performance in simulating the spatial distribution of temperature as compared with other variables, which has already been partly documented (Zhao et al., 1995; Jiang et al., 2005; Xu et al., 2007). It is notable that almost all of the models' SCC values exceed 0.97, and the RAE values vary from –3.489°C (UKMO-HadGE-

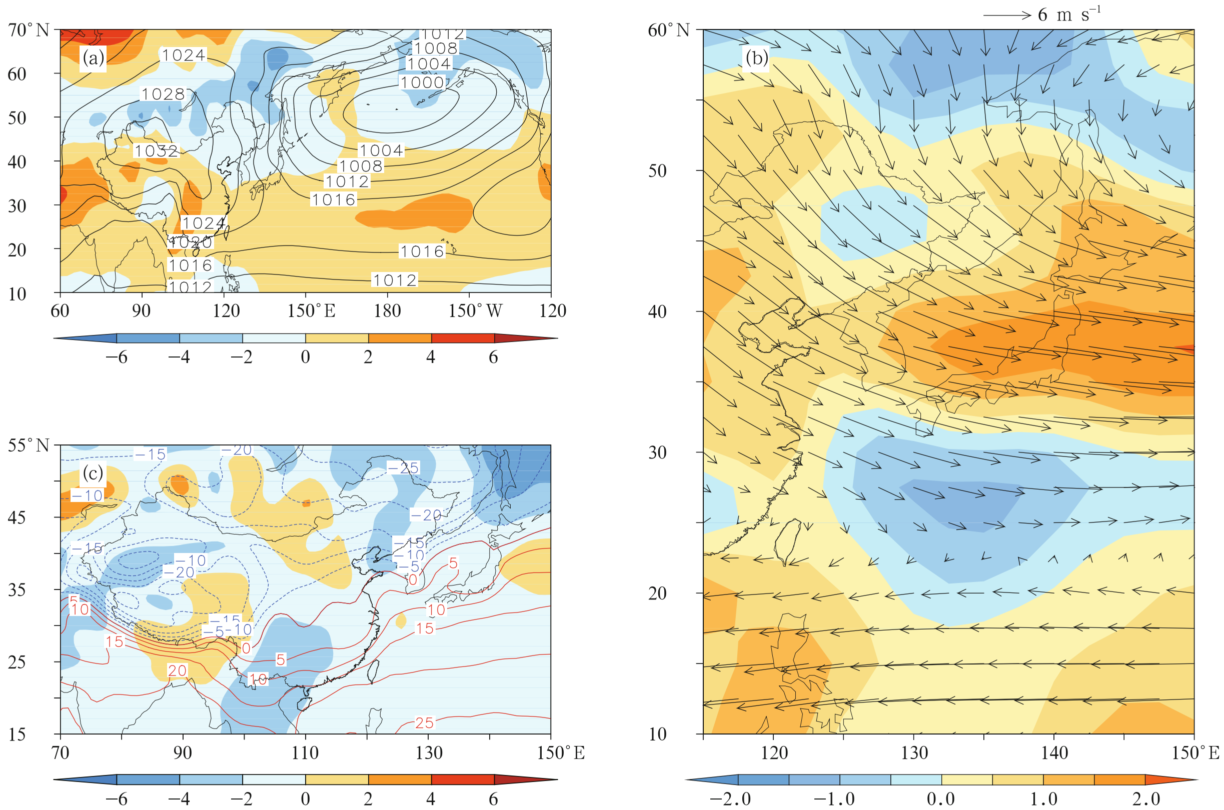

Fig. 1. Climatology of (a) sea level pressure (SLP; hPa), (b) wind at 850 hPa (uv_{850}; m s^{-1}), and (c) surface air temperature (SAT; ℃) for the winters of 1960–1998 as simulated by the multi-model ensemble. The nine-point running average differences between the ensemble mean and observations are shaded.

M1) to 1.550℃ (CSIRO-MK3.5). The underestimation by 13 of the 20 models as well as that of the multi-model ensemble mean indicates a cooling bias of the current coupled models (Jiang et al., 2005; Xu et al., 2007; Liu and Jiang, 2009). However, the significant spatial correlation coefficient (0.996) for the 20-model ensemble mean is impressive.

Based on the above analysis, we can confidently approve the current coupled models' performance in simulating the climatology of the EAWM. However, in practical application, more attention is given to their validations in reproducing the evolution of circulation and other meteorological elements. Thus, the decadal and interdecadal variations of the EAWM-related atmospheric general circulation will be discussed in the following two sections, respectively.

4. Assessment of model performance in simulating the decadal EAWM variations

An important characteristic of the EAWM on the decadal timescale is its continuous weakening since 1986 (Kang et al., 2006; Yan et al., 2009; Wang and Chen, 2010). Although the EAWM is a regional phenomenon, its variation correlates well with the change of large-scale circulation (Wang and Jiang, 2004). From this point of view, EAWM-related atmospheric general circulation must have changed greatly between 1980 and 1989. To quantitatively evaluate the models' performance in this regard, the observed and simulated linear trends of sea level pressure (SLP) and geopotential height at 500 hPa (H500) for the period of 1980–1989 are estimated with linear regression (Fig. 2). The coefficients of spatial correlation between the observed and simulated linear trends in the Northern Hemisphere are displayed in Table 2.

In the observed SLP field, there are decreasing trend varying from −0.3 to −1.2 hPa yr^{-1} in high latitudes and increasing trends of 0.3–1.2 hPa yr^{-1} elsewhere, in particular, western Europe and the North Pacific, resulting in a "+ − +" tripolar pattern (Fig. 2a). This means that the Arctic oscillation (AO) was enhanced and that the SH and AL were weakened in the boreal winters of 1980–1989. As expected, the models did not show the same performance in simulating the decadal variations as in reproducing the climatology (the second column of Table 2). However, considering the large sample grids, all of the positive SCC should be valid. There are 10 models, i.e., BCCR-BCM2.0, CCSM3, CGCM3.1 (T63), CNRM-CM3 (Centre National de Researches Météorologiques Coupled Global Climate Model version 3), CSIRO-MK3.0, GFDL-CM2.1, INGV-ECHAM4, MIROC3.2 (medres), MIROC3.2 (hires), and ECHAM5/MPI-OM, producing SCCs at the 5% significance level. Consequently, the improvement of the 10-model ensemble is remarkable, with the SCC reaching 0.676. As shown in Fig. 2b, the 10-model ensemble correctly shows increasing trends in western Europe and the North Pacific as well as decreasing trends in Siberia and North Atlantic. Unfortunately, the amplitude is underestimated.

In pace with the changing SLP, H500 also exhibited obvious decadal variability during the winters of 1980–1989. As illustrated in Fig. 2c, three prominent positive ascending trend centers are observed in western Europe, from East Asia to North Pacific, and southern North America, respectively. At the same time, three evident negative centers are found emerging in the Ural Mountains, Bering Sea, and North Atlantic. All of the above, to a certain extent, suggests a weakening of the East Asian trough, an enhancement of the North Atlantic Oscillation (NAO), and a deepening of the Polar vortex. The values listed in the third column of Table 2 indicate that 13 coupled models, i.e., BCCR-BCM2.0, CCSM3, CGCM3.1 (T63), CNRM-CM3, CSIRO-MK3.0, GFDL-CM2.1, GISS-ER, INM-CM3.0, MIROC3.2 (medres), MIROC3.2 (hires), ECHAM5/MPI-OM, MRI-CGCM2.3.2 (Meteorological Research Institute Coupled Global Climate Model version 2.3.2), and UKMO-HadCM3 (Hadley Centre Coupled Ocean-Atmosphere General Circulation Model version 3), have simulated the above spatial variational pattern reasonably well. When taking into account these 13 models, the multi-model ensemble mean again shows encouraging results (Fig. 2d), with a spatial correlation coefficient of 0.801. It is notable that the above-mentioned negative and positive centers' locations and ranges are accurately reproduced by the 10-model ensemble. However, the problem of underestimated amplitude, which is approximately one third of the observation, remains. In addition, the ability of the CSIRO-MK3.0 to reproduce the decadal variations of the circulation is the best. In contrast, CGCM3.1 (T47) gives relatively larger simulation errors, the spatial pattern of which is almost opposite to that of the observation.

Because the intensity of the EAWM experienced a moderate declining trend (Yan et al., 2009), we further analyze the linear trends of an EAWM index for 1980–1989. The linear trend of the area-averaged 500-hPa geopotential height anomalies in the domain of 25°–40°N, 110°–155°E, which is defined as the EAWM index, for the observations and simulations, is shown

Table 2. Coefficients of spatial correlation between the observed and simulated linear trends of SLP and H500 in the Northern Hemisphere for the winters of 1980–1989

Model	SLP	H500
BCCR-BCM2.0	**0.179**	**0.235**
CCSM3	**0.337**	**0.383**
CGCM3.1 (T47)	–0.418	–0.323
CGCM3.1 (T63)	**0.443**	**0.557**
CNRM-CM3	**0.255**	**0.386**
CSIRO-MK3.0	**0.499**	**0.559**
CSIRO-MK3.5	–0.366	–0.150
GFDL-CM2.0	–0.386	–0.362
GFDL-CM2.1	**0.355**	**0.442**
GISS-ER	–0.171	**0.231**
INGV-ECHAM4	**0.069**	–0.047
INM-CM3.0	–0.067	**0.069**
IPSL-CM4	–0.221	–0.021
MIROC3.2 (medres)	**0.305**	**0.256**
MIROC3.2 (hires)	**0.292**	**0.328**
ECHAM5/MPI-OM	**0.185**	**0.186**
MRI-CGCM2.3.2	–0.016	**0.075**
PCM1	–0.207	–0.036
UKMO-HadCM3	–0.008	**0.090**
UKMO-HadGEM1	–0.020	–0.215
Ensemble mean*	**0.676**	**0.801**

* Only takes into account the models exceeding the 5% significance level. SLP: sea level pressure; H500: 500-hPa geopotential height. The bold values are statistically significant at the 5% level.

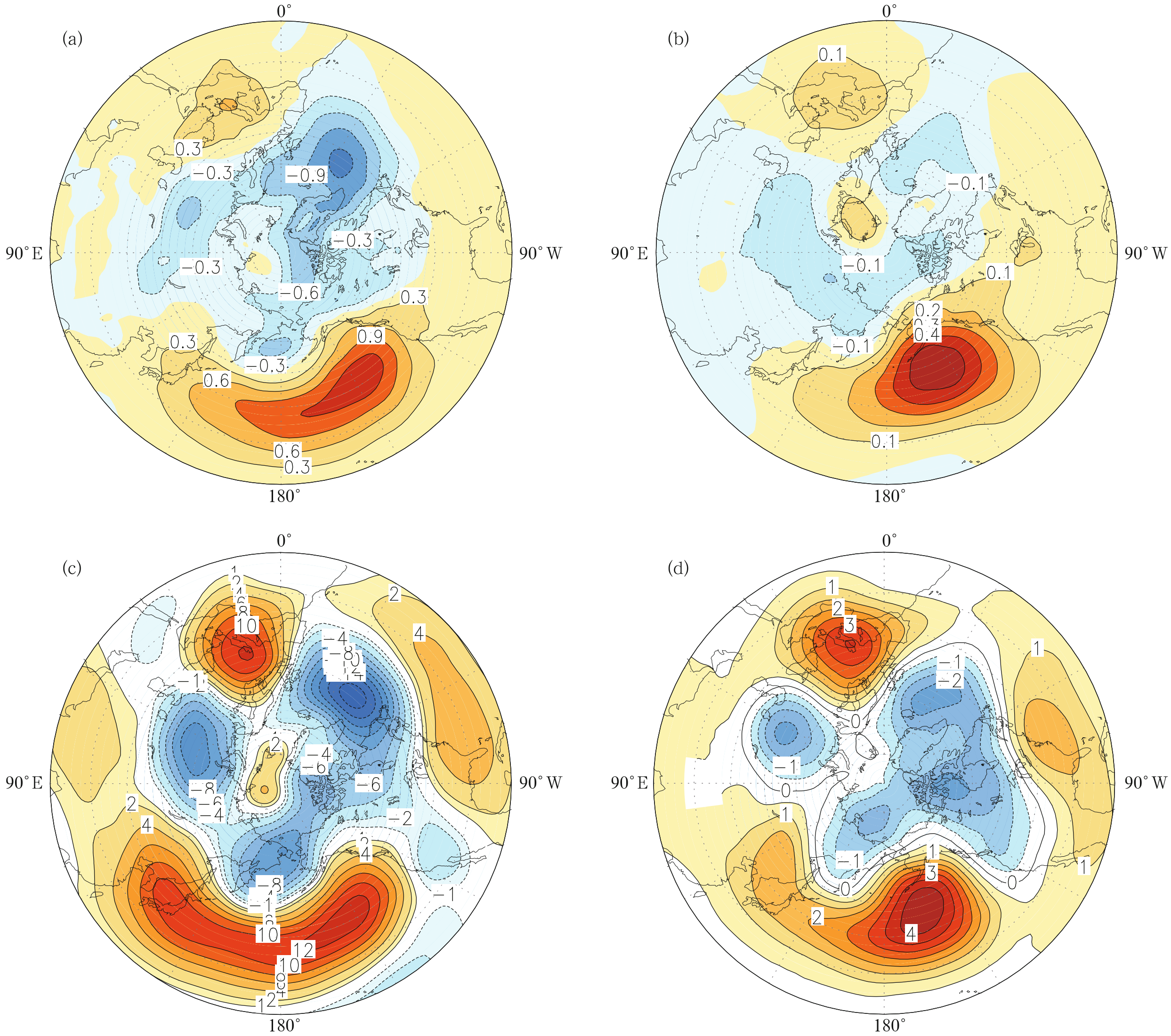

Fig. 2. Linear trends of (a, b) sea level pressure (hPa yr^{-1}) and (c, d) 500-hPa geopotential height (gpm yr^{-1}) for the winters of 1980–1989 north of 20°N obtained from observations (a, c) and the ensemble mean of selected coupled climate models (b, d).

in Fig. 3. There is an increasing trend of 7 gpm yr^{-1}, indicating a pronounced weakening of the EAWM intensity. The observed declining trend is successfully reproduced by most of the models, although the simulated amplitudes are far underestimated from the observations. Only four models (CGCM3.1-T47, CNRM-CM3, GFDL-CM2.0, and UKMO-HadGEM1) failed to simulate the observed declining trend of the EAWM index.

5. Assessment of model performance in simulating the interdecadal EAWM variations

The EAWM is characterized by obvious interannual variability as well as interdecadal variability (Shi, 1996; Jhun and Lee, 2004; Wang et al., 2009). Because the EAWM experienced a significant shift around 1986 (Yan et al., 2009; Wang and Chen, 2010), in the following assessment, we use 1960–1985 and 1986–1998 to represent the strong and weak EAWM periods, respectively. Figure 4a (4c) illustrates the observed differences in SLP (H500) between the strong and weak EAWM periods. The negative and positive phases of the SLP anomalies are separated by approximately 45°N in the Northern Hemisphere (Fig. 4a). In the high latitudes, the anomalies are generally greater than –1 hPa, with the largest values located in Green-

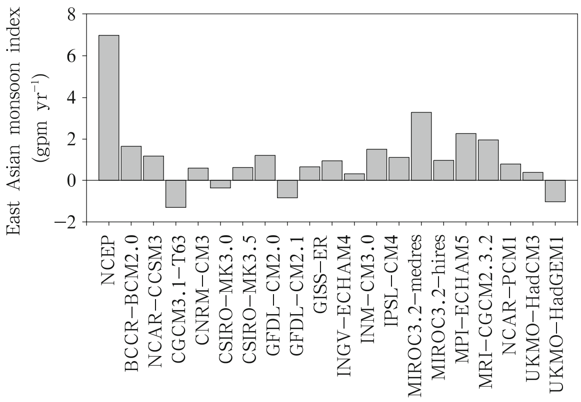

Fig. 3. Linear trends of the East Asian monsoon index (area-averaged H500 anomalies in the domain of 25°–40°N, 110°–155°E) from observations (NCEP) and 20 coupled climate models for 1980–1989 (unit: gpm yr^{-1}).

land and west of Siberia, where the anomalies reach –4 hPa or even more. From the perspective of the EAWM, the SH and AO are both weakened in the later period. Meanwhile, in the subtropical area, the SLP rises by 1–3 hPa, showing three positive centers in southern Europe, western China, and the North Pacific, respectively. Thus, it is suggested that the AL is also weakened. This result is consistent with that of a previous study (Wang et al., 2009). At a large circulation scale, the overall SLP distribution indicates that the NAO and the North Pacific Oscillation (NPO) are intensified as well. At the same time, the H500 displays an interdecadal variation distribution similar to that of the SLP (Fig. 4c). All of the factors mentioned above favor a weakening of the EAWM.

To evaluate the capacity of individual models to simulate the interdecadal changes of SLP, the coefficients of spatial correlation between the observed and simulated SLP anomalies for each individual model are displayed in the second column of Table 3. It is shown that 10 of the 20 models, i.e., BCCR-BCM2.0, CGCM3.1(T63), CNRM-CM3, CSIRO-MK3.0, CSIRO-MK3.5, GISS-ER, INM-CM3.0, MRI-CGCM2.3.2, PCM1, and UKMO-HadGEM1, have significant correlation, among which, CNRM-CM3, INM-CM3.0, MRI-CGCM2.3.2, and PCM1 have relatively high reproducibility, with spatial correlation coefficients reaching 0.606, 0.660, 0.682, and 0.684, respectively. In addition, the above 10-model ensemble exhibits an even better score (0.814). Figure 4b shows the 10-model ensemble mean of the SLP anomalies. The simulated spatial distribution of the interdecadal change is in accord with the reanalysis data overall, with negative anomalies in the mid and high latitudes and positive anomalies in the low latitudes. The reproduction of the ascending trend centers located in southern Europe and the North Pacific are most encouraging. All of the above denotes that the ensemble mean can reasonably reproduce the weakening trend of the SH and AL as well as the intensifying trend of the AO, NAO, and NPO, demonstrating the ability of the models to simulate the interdecadal variations of the EAWM. Unfortunately, the range of the simulation values is still smaller than that of the observation.

The values in the third column of Table 3 indicate that there is one more model, i.e., CGCM3.1 (T47), that can reasonably capture the H500 interdecadal anomalies of 1960–1985 and 1986–1998 in addition to the above 10 mentioned models. Consequently, the ensemble mean here will take into account these 11 models. In general, the 11-model ensemble mean exhibits much better performance than any individual

Table 3. Coefficients of spatial correlation between the observed and simulated interdecadal variations (1986–1998 minus 1960–1985) of SLP and H500 in the Northern Hemisphere

Model	SLP	H500
BCCR-BCM2.0	**0.213**	**0.158**
CCSM3	–0.571	–0.539
CGCM3.1 (T47)	–0.003	**0.056**
CGCM3.1 (T63)	**0.285**	**0.302**
CNRM-CM3	**0.606**	**0.550**
CSIRO-MK3.0	**0.425**	**0.321**
CSIRO-MK3.5	**0.445**	**0.201**
GFDL-CM2.0	–0.390	–0.481
GFDL-CM2.1	–0.369	–0.263
GISS-ER	**0.532**	**0.498**
INGV-ECHAM4	–0.379	–0.343
INM-CM3.0	**0.660**	**0.512**
IPSL-CM4	–0.040	–0.066
MIROC3.2 (medres)	–0.386	–0.358
MIROC3.2 (hires)	–0.148	–0.208
ECHAM5/MPI-OM	–0.446	–0.283
MRI-CGCM2.3.2	**0.682**	**0.647**
PCM1	**0.684**	**0.385**
UKMO-HadCM3	–0.121	–0.102
UKMO-HadGEM1	**0.401**	**0.287**
Ensemble mean*	**0.814**	**0.808**

* Only takes into account the models exceeding the 5% significance level. SLP: sea level pressure; H500: 500-hPa geopotential height. The bold values are statistically significant at the 5% level.

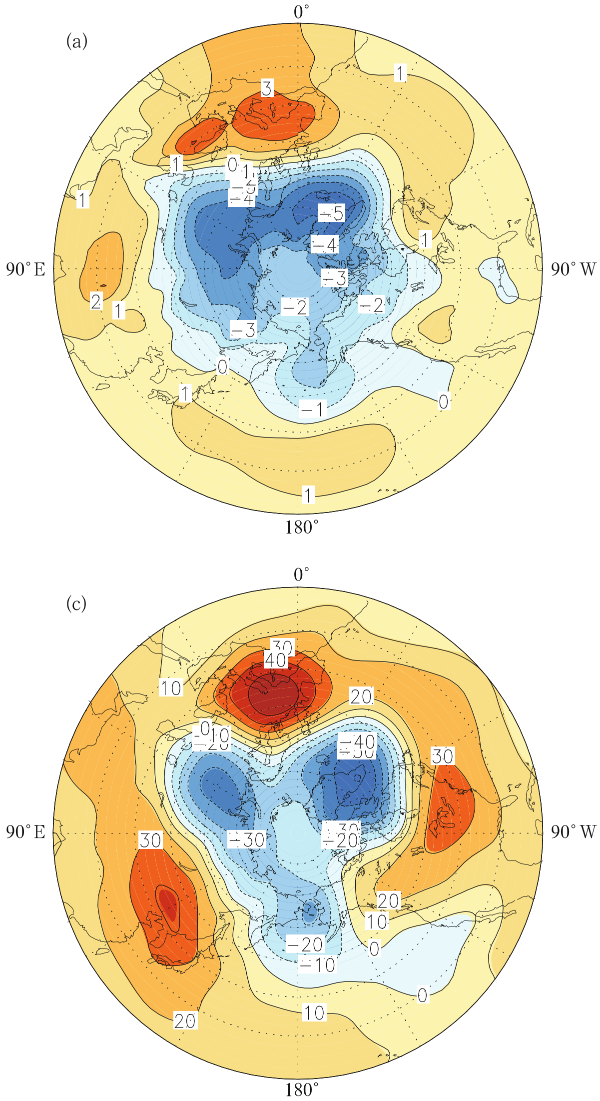

Fig. 4. Interdecadal change (1986–1998 minus 1960–1985) in (a, b) SLP (hPa) and (c, d) H500 (gpm) from (a, c) observations and (b, d) the ensemble mean of selected coupled models.

model, with a spatial correlation coefficient as high as 0.808. As is shown in Fig. 4d, the ensemble mean shows three positive anomaly centers in southern Europe, East Asia, and southern North America, which also emerged in the observation (as illustrated in Fig. 4c). It should be noted that the second positive center is located where the East Asian trough generally appears, which again demonstrates that the coupled models can reflect the interdecadal variations of EAWM-related circulation. On the other hand, a negative phase in the polar region is shown for the 11-model ensemble mean, which agrees with the observation. However, the variational magnitude is underestimated. Furthermore, the ensemble mean anomalies over 60°–70°N are almost opposite to the observations. As a result, the observed negative anomalies in Siberia, Northwest Pacific, and North Atlantic are not well reproduced by the 11-model ensemble mean. Additionally, MRI-CGCM2.3.2 is the best model for describing the interdecadal changes in H500, followed by CNRM-CM3. Comparatively, the performances of CCSM3 and GFDL-CM2.0 are slightly worse than those of the other models.

6. Discussion and conclusions

The boreal winter climatology of the East Asian SLP, 850-hPa wind, and SAT, the decadal variations of the EAWM and EAWM-related circulation, and the interdecadal variations of EAWM-related circulation, as simulated by 20 coupled atmosphere-ocean models, were systematically evaluated on the basis of the NCEP reanalysis data. The primary conclusions are as follows.

(1) The models can successfully reproduce the geographical distribution of the East Asian SLP, 850-hPa wind, and SAT. In general, the best performance is exhibited for the SAT. In terms of intensity, the 850-hPa wind is generally overestimated and the SLP and SAT are underestimated by the coupled models. Comparatively, the current state-of-the-art coupled models exhibit relatively better performance in simulating spatial variations over flat terrain than over complex topography.

(2) Ten models reproduced the decadal variations of SLP reasonably well for the boreal winters of 1980–1989. The 10-model ensemble mean successfully reproduced the weakening trends of the SH and AL as well as the intensifying trend of the Arctic Oscillation. In addition, 13 models reasonably simulated the decadal variations of H500 for 1980–1989. The weakening of the East Asian trough, the strengthening of the NAO, and the deepening of the Polar vortex were all successfully reproduced by the 13-model ensemble. Furthermore, CSIRO-MK3.0 exhibited the best performance in simulating the decadal variations of the EAWM-related circulation. Unfortunately, the variational magnitude is only weakly comparable to the observation.

(3) The observed declining trend of the EAWM intensity was successfully reproduced by most of the models although the simulated amplitudes are far underestimated from the observations. Only 4 models (CGCM3.1-T47, CNRM-CM3, GFDL-CM2.0, and UKMO-HadGEM1) failed to simulate the observed declining trend of the EAWM index.

(4) It was found that 10 of the 20 models captured the main spatial distribution of SLP differences between 1960–1985 and 1986–1998, among which CNRM-CM3, INM-CM3.0, MRI-CGCM2.3.2, and PCM1 have relatively high reproducibility, with spatial correlation coefficients reaching 0.606, 0.660, 0.682, and 0.684, respectively. The above 10-model ensemble mean exhibited an even better score (0.814). It is noted that the 10-model ensemble mean can reasonably reproduce the weakening trends of the SH and AL as well as the intensifying trend of the AO, NAO, and NPO, showing its ability to simulate the interdecadal variation of the EAWM. In addition to the above 10 coupled models, there is one more model (CGCM3.1 (T47)) that can reproduce the 500-hPa geopotential height interdecadal anomalies reasonably well for 1960–1985 and 1986–1998. Although the 11-model ensemble mean reasonably reproduced the positive anomalies in the low latitudes as well as the negative anomalies in the polar region, the simulated anomalies for 60°–70°N are almost opposite to the observations. Additionally, the amplitude was still underestimated.

To objectively investigate the performance of each individual coupled model in simulating the variations of the EAWM, we did not choose the same models for the multi-model ensemble mean. However, it is obvious that BCCR-BCM2.0, CGCM3.1-T63, CNRM-CM3, CSIRO-MK3.0, GISS-ER, INM-CM3.0, and MRI-CGCM2.3.2 exhibited better performance in every aspect, even though there still exist uncertainties to a certain degree. Thus, one should pay more attention to these models when trying to use the above models' outputs to address or forecast variations of the East Asian winter monsoon. In addition, the complex physical reasons behind the models' performance were not examined in detail. We think a better dynamical framework or a higher resolution may contribute to an encouraging simulation. For example, the dynamical framework is the only difference between GFDL-CM2.0 and GFDL-CM2.1, while CGCM3.1 (T63) has a higher horizontal resolution than CGCM3.1 (T47). The result is that GFDL-CM2.1 and CGCM3.1 (T63) have better performance than GFDL-CM2.0 and CGCM3.1 (T47), respectively. However, further efforts should be devoted to determining the mechanism governing the variations of the EAWM.

REFERENCES

Annamalai, H., K. Hamilton, and K. R. Sperber, 2007: South Asian summer monsoon and its relationship with ENSO in the IPCC AR4 simulations. *J. Climate*, **20**, 1071–1083.

Bollasina, M., and S. Nigam, 2009: Indian Ocean SST, evaporation, and precipitation during the South Asian summer monsoon in IPCC-AR4 coupled simulations. *Climate Dyn.*, **33**(7), 1017–1032.

Buhe, C., C. Ulrich, Y. H. Lin, et al., 2003: The change of North China climate in transient simulations using the IPCC SRES A2 and B2 scenarios with a coupled atmosphere-ocean general circulation model. *Adv. Atmos. Sci.*, **20**(5), 755–766.

Chen Juan and Sun Shuqing, 1999: East Asian winter monsoon anomaly and variation of global circulation. Part I: A comparison study on strong and weak winter monsoons. *Chinese J. Atmos. Sci.*, **23**(1), 101–111. (in Chinese)

Chen, W., S. Yang, and R. H. Huang, 2005: Relationship between stationary planetary wave activity and the East Asian winter monsoon. *J. Geophys. Res.*, **110**, D14110, doi: 10.1029/2004JD005669.

Dai, A. G., 2006: Precipitation characteristics in eighteen coupled climate models. *J. Climate*, **19**(18), 4605–4630.

Feng Jinming and Fu Congbin, 2007: Inter-comparison of long-term simulations of temperature and precipitation over China by different regional cliamte models. *Chinese J. Atmos. Sci.*, **31**(5), 805–814. (in Chinese)

Gao Xuejie, Ding Yihui, Zhao Zongci, et al., 2003a: Climate change due to greenhouse effects in China as simulated by a regional climate model. Part I: Evaluation of the model simulations. *Acta Meteor. Sinica*, **61**(1), 21–27. (in Chinese)

—,—, —, et al., 2003b: Cliamte change due to greenhouse effects in China as simulated by a regional climate model. Part II: Climate change. *Acta Meteor. Sinica*, **61**(1), 29–38. (in Chinese)

—, Lin Wantao, F. Kucharsky, et al., 2004: A simulation of regional climate in China by using CCM3 and observed SST. *Chinese J. Atmos. Sci.*, **28**(1), 78–90. (in Chinese)

Gong Daoyi, Zhu Jinhong, and Wang Shaowu, 2002: The influence of Siberian high on large-scale climate over continental Asia. *Plateau Meteor.*, **21**(1), 8–14. (in Chinese)

Gu Wei and Li Chongyin, 2010: Evaluation of the IPCC AR4 climate models in simulating the interdecadal variations of the East China summer precipitation, PDO and NAO. *Trans. Atmos. Sci.*, **33**(4), 401–411. (in Chinese)

Guo Qiyun, 1994: Relationship between the variations of East Asian winter monsoon and temperature anomalies in China. *J. Appl. Meteor. Sci.*, **5**(2), 218–225. (in Chinese)

Jhun, J. G., and E. J. Lee, 2004: A new East Asian winter monsoon index and associated characteristics of the winter monsoon. *J. Climate*, **17**, 711–726.

Ji, L. R., and S. Q. Sun, 1997: Model study on the interannual variability of Asian winter monsoon and its influence. *Adv. Atmos. Sci.*, **14**(1), 1–22.

Jiang, D. B., 2008: Projected potential vegetation change in China under the SRES A2 and B2 scenarios. *Adv. Atmos. Sci.*, **25**(1), 126–138.

—, H. J. Wang, and X. M. Lang, 2005: Evaluation of East Asian climatology as simulated by seven coupled models. *Adv. Atmos. Sci.*, **22**(4), 479–495.

Jiang Zhihong, Chen Weilin, Song Jie, et al., 2009: Projection and evalutation of the precipitation extreme indices over China based on seven IPCC AR4 coupled climate models. *Chinese J. Atmos. Sci.*, **33**(1), 109–120. (in Chinese)

Kalnay, E., M. Kanamistsu, R. Kistler, et al., 1996: The NCEP/NCAR Reanalysis Project. *Bull. Amer. Meteor. Soc.*, **77**, 437–470.

Kang Lihua, Chen Wen, and Wei Ke, 2006: The interdecadal variation of winter temperature in China and its relation to anomalies in atmospheric general circulaion. *Climatic Environ. Res.*, **11**, 330–339. (in Chinese)

Kripalani, R. H., J. H. Oh, and H. S. Chaudhari, 2007a: Response of the East Asian summer monsoon to doubled atmospheric CO_2: Coupled climate model simulations and projections under IPCC AR4. *Theor. Appl. Climatol.*, **87**, 1–28.

—, A. Kulkarni, et al., 2007b: South Asian summer monsoon precipitation variability: Coupled climate model simulations and projections under IPCC AR4. *Theor. Appl. Climatol.*, **90**(3), 133–159.

Lambert, S. J., and G. J. Boer, 2001: CMIP1 evaluation and intercomparison of coupled climate models. *Climate Dyn.*, **17**, 83–106.

Lin, J. L., N. K. George, E. M. Brian, et al., 2006: Tropical intraseasonal variability in 14 IPCC AR4 climate models. Part I: Convective signals. *J. Climate*, **19**, 2665–2690.

——, M. W. Klaus, N. K. George, et al., 2008: Subseasonal variability associated with Asian summer monsoon simulated by 14 IPCC AR4 coupled GCMs. *J. Climate*, **21**, 4541–4567.

Liu Min and Jiang Zhihong, 2009: Simulation ability evaluation of surface temperature and precipitation by thirteen IPCC AR4 coupled climate models in China during 1961–2000. *J. Nanjing Institute of Meteorology*, **32**(2), 256–268. (in Chinese)

Min, S.-K., E.-K. Park, and W.-T. Kwon, 2004: Future projections of East Asian climate change from multi-AOGCM ensemble of IPCC SERS scenario simulations. *J. Meteor. Soc. Japan*, **82**(4), 1187–1211.

Shi Neng, 1996: Features of the East Asian winter monsoon intensity on multiple time scales in recent 40 years and their relation to climate. *J. Appl. Meteor. Sci.*, **7**, 175–182. (in Chinese)

Sun Yin and Ding Yihui, 2008: An assessment on the performance of IPCC AR4 climate models in simulating interdecadal variations of the East Asian summer monsoon. *Acta Meteor. Sinica*, **22**(5), 472–488.

Tao Shiyan and Chen Longxun, 1987: A review of recent research on the East Asian monsoon in China. *Monsoon Meteorology.* Oxford University Press, 60–92.

Wang Huijun, Lang Xianmei, Zhou Guangqing, et al., 2003: A preliminary report of the model prediction on the forthcoming winter and spring dust cliamte over China. *Chinese J. Atmos. Sci.*, **27**(1), 134–140. (in Chinese)

—— and Jiang Dabang, 2004: A new East Asian winter monsoon intensity index and atmospheric circulation comparison between strong and weak composite. *Quaternary Sciences*, **24**(1), 19–27. (in Chinese)

Wang, L., R. H. Huang, L. Gu, et al., 2009: Interdecadal variations of the East Asian winter monsoon and their association with quasistationary planetary wave activity. *J. Climate*, **22**, 4860–4872.

——, and W. Chen, 2010: How well do existing indices measure the strength of the East Asian winter monsoon? *Adv. Atmos. Sci.*, **27**(4), 855–870.

Wang Shiyu and Zhang Yaocun, 1999: Simulation of regional cliamte over eastern China with different regional cliamte models. *Plateau Meteor.*, **18**(1), 28–38. (in Chinese)

Wang Shuyu and Xiong Zhe, 2004: The preliminary analysis of 5 coupled ocean-atmosphere global climate models simulation of regional climate in Aisa. *Climatic Environ. Res.*, **9**(2), 240–250. (in Chinese)

Xu Chonghai, Shen Xinyong, and Xu Ying, 2007: An analysis of climate change in East Asia by using the IPCC AR4 simulations. *Adv. Climate Change Res.*, **3**(5), 287–292. (in Chinese)

Xu Ying, Ding Yihui, and Zhao Zongci, 2002: Detection and evaluation of effect of human activities on climatic change in East Asia in recent 30 years. *J. Appl. Meteor. Sci.*, **13**(5), 513–525. (in Chinese)

Yan Hongming, Zhou Wen, Yang Hui, et al., 2009: Definition of a East Asian winter monsoon index and its variation characteristics. *Trans. Atmos. Sci.*, **32**(3), 367–376. (in Chinese)

Zhao Ping and Zhang Renhe, 2006: Relationship of interannual variation between an eastern Asia-Pacific dipole pressure and East Asian monsoon. *Chinese J. Atmos. Sci.*, **30**(2), 307–316. (in Chinese)

Zhao Zongci, Ding Yihui, Li Xiaodong, et al., 1995: Evaluation of CGCM climate simulation in East Asian region. *J. Appl. Meteor. Sci.*, **6**(1), 9–18. (in Chinese)

——, Xu Ying, et al., 2003: Detection and prediction of climate change for the 20th and 21st century due to human activity in Northwest. *Climatic Environ. Res.*, **8**(1), 26–34. (in Chinese)

Zhou Baotao, He Jinhai, Chen Longxun, et al., 2004: Climatological assessment on basic simulation results of GISS atmosphere-ocean coupled model China. *J. Appl. Meteor. Sci.*, **15**(4), 500–505. (in Chinese)

Zhou, T. J., and Z. X. Li, 2002: Simulation of the East Asian summer monsoon using a variable resolution atmospheric GCM. *Climate Dyn.*, **19**, 167–180.

——, and R. C. Yu, 2006: Twentieth-century surface air temperature over China and the globe simulated by coupled climate models. *J. Climate*, **19**(22), 5843–5858.